

# The Host Galaxy of GRB 990712<sup>\*,\*\*</sup>

Lise Christensen<sup>1</sup>, Jens Hjorth<sup>2</sup>, Javier Gorosabel<sup>3,4,5</sup>, Paul Vreeswijk<sup>6,7</sup>, Andrew Fruchter<sup>8</sup>, Kailash Sahu<sup>8</sup>, and Larry Petro<sup>8</sup>

<sup>1</sup> Astrophysikalisches Institut Potsdam, An der Sternwarte 16, 14482 Potsdam, Germany

<sup>2</sup> Niels Bohr Institute, Astronomical Observatory, University of Copenhagen, Juliane Maries Vej 30, 2100 Copenhagen Ø, Denmark

<sup>3</sup> Instituto de Astrofísica de Andalucía, IAA-CSIC, Granada, Spain

<sup>4</sup> Laboratorio de Astrofísica Espacial y Física Fundamental (LAEFF-INTA), P.O. Box 50727, 28080, Madrid, Spain

<sup>5</sup> Danish Space Research Institute, Juliane Maries Vej 30, 2100 Copenhagen Ø, Denmark

<sup>6</sup> European Southern Observatory, Casilla 19, Santiago, Chile

<sup>7</sup> Astronomical Institute "Anton Pannekoek", University of Amsterdam & Center for High Energy Astrophysics, Kruislaan 403, 1098 SJ Amsterdam, The Netherlands

<sup>8</sup> Space Telescope Science Institute, 3700 San Martin Drive, Baltimore, MD 21218.

Received / Accepted

**Abstract.** We present a comprehensive study of the  $z = 0.43$  host galaxy of GRB 990712, involving ground-based photometry, spectroscopy, and HST imaging. The broad-band *UBVRIZJKs* photometry is used to determine the global spectral energy distribution (SED) of the host galaxy. Comparison with that of known galaxy types shows that the host is similar to a moderately reddened starburst galaxy with a young stellar population. The estimated internal extinction in the host is  $A_V = 0.15 \pm 0.1$  and the star-formation rate (SFR) from the UV continuum is  $1.3 \pm 0.3 M_{\odot} \text{ yr}^{-1}$  (not corrected for the effects of extinction). Other galaxy template spectra than starbursts failed to reproduce the observed SED. We also present VLT spectra leading to the detection of  $H\alpha$  from the GRB host galaxy. A SFR of  $2.8 \pm 0.7 M_{\odot} \text{ yr}^{-1}$  is inferred from the  $H\alpha$  line flux, and the presence of a young stellar population is supported by a large equivalent width. Images from HST/STIS show that the host has two separate knots, which could be two distinct star-forming regions.

**Key words.** gamma rays: bursts – galaxies: hosts – galaxies: star formation

## 1. Introduction

For all but one of the Gamma-Ray Bursts (GRBs) where the position of the X-ray, optical, or radio afterglow has been localised to an accuracy of less than  $1''$ , follow-up deep observations have revealed underlying galaxies. The current sample consists of  $\sim 45$  such GRB hosts, and  $\sim 35$  of these have measured redshifts in the range  $0.168 < z < 4.5$  (Hjorth et al. 2003; Andersen et al. 2000) and have magnitudes  $21 < R < 30$ . The faintness of the hosts requires long integration times on the largest telescopes to obtain high signal

to noise ratio spectra. Ground-based broad-band photometry presents a useful alternative for investigating the spectral energy distribution (SED).

The relatively small size of GRB hosts sometimes makes it difficult to tell which morphological type it is, e.g. whether the radial intensity profile of the galaxy is best fitted by an exponential disk profile or an elliptical profile. However, studies of some hosts with the HST have shown that an exponential profile provides a good fit to the surface intensity distribution (Odewahn et al. 1998; Fruchter et al. 2000; Hjorth et al. 2002). Comparing the SED of the host with the SEDs of known galaxy types provides an alternate method of estimating the galaxy type. Sokolov et al. (2001) analysed 6 GRB hosts in this way, showing that all of them had SEDs characteristic of starburst galaxies. This is expected if GRBs are associated with massive collapsing stars as suggested by Woosley (1993) and Wijers et al. (1998) and recently observed for the GRB 030329 (Stanek et al. 2003; Hjorth et al. 2003). A small age for the burst population gives an indication that GRB progenitors are massive stars, whereas SED ages much longer than the life times of the

\* Based on observations collected at the European Southern Observatory, La Silla, with the ESO 3.6m telescope, NTT, and VLT (ESO Programmes 165.H-0464(I) and 165.H-0464(E), and 265.D-5742(B)) by the Gamma-Ray Burst Afterglow Collaboration at ESO (GRACE) group. Further based on observations with the Danish 1.5m telescope.

\*\* Based on observations with the NASA/ESA Hubble Space Telescope, obtained at the Space Telescope Science Institute, which is operated by the Association of Universities for Research in Astronomy, Inc. under NASA contract NAS5-26555.

Correspondence to: lchristensen@aip.de

most massive stars could indicate a binary merging event as the cause of the GRB (Eichler et al. 1989).

The GRB 990712 host is bright relative to other GRB hosts, and therefore serves as a good case for studying the multi-band SED. This paper is one in a series of papers on the SEDs of GRB hosts. Studies of the hosts of GRB 000210 and GRB 000418 are presented in Gorosabel et al. (2003a) and Gorosabel et al. (2003b), respectively.

The previous studies of the GRB 990712 afterglow and the host are summarised in Sect. 2. In Sect. 3 and Sect. 4 we present photometry and spectroscopy of the GRB 990712 host. The morphology of the host is investigated in Sect. 5. A comparison of the SED derived from all the observations with spectral synthetic templates is described in Sect. 6. In Sect. 7 we estimate the SFR of the host galaxy using two SFR estimators; first using the UV continuum and second the  $H\alpha$  line flux. In Sect. 8 we discuss the results.

Throughout the paper we assume  $\Omega_m = 0.3$ ,  $\Omega_\Lambda = 0.7$  and  $H_0 = 65 \text{ km s}^{-1} \text{ Mpc}^{-1}$ . At the redshift of the host,  $z = 0.433$ , the luminosity distance is  $d_L = 7.93 \times 10^{27} \text{ cm}$ .

## 2. GRB 990712

GRB 990712 was detected on July 12 1999 at UT 16:43:02, by the Italian-Dutch satellite BeppoSAX (Frontera 1999). The burst had the strongest afterglow observed in X-rays to that date. Its afterglow was found approximately 4 hours after the trigger by Bakos et al. (1999). A spectrum obtained shortly after revealed a redshift of  $z = 0.433$  from the emission lines [O II], [O III],  $H\gamma$  and  $H\beta$  as well as Mg I and Mg II absorption lines (Galama et al. 1999; Hjorth et al. 2000). The relatively low redshift makes it one of the closest GRB hosts. Only the GRB 980425 at  $z = 0.0085$  (Galama et al. 1998), GRB 011121 at  $z = 0.36$  (Infante et al. 2001) and GRB 030329 at  $z = 0.168$  (Greiner et al. 2003) were nearer.

A spectrum of the combined flux from the host and the afterglow was obtained by Vreeswijk et al. (2001a) 1.5 days after the burst. Because of the brightness of the host, the spectrum shows distinct absorption lines and emission lines from the host itself.

The [O II] emission line flux was measured to be  $(3.37 \pm 0.2) \times 10^{-16} \text{ erg cm}^{-2} \text{ s}^{-1}$  (Vreeswijk et al. 2001a), which corresponds to a SFR of  $2.7 \pm 0.8 M_\odot \text{ yr}^{-1}$  using the conversion from measured flux to a SFR from Kennicutt (1998) (Hereafter K98). Converting the flux at restframe 2800 Å to a SFR gives a similar result. An internal extinction of  $A_V = 3.4_{-1.7}^{+2.4}$  was inferred from the flux ratio of the hydrogen lines  $H\gamma/H\beta$ . The host was observed at radio frequencies (1.4 GHz) by Vreeswijk et al. (2001b), who did not find any radiation from the host to a limit of  $70 \mu\text{Jy}$ . This upper limit implies that the total unextincted SFR in the host is less than  $100 M_\odot \text{ yr}^{-1}$ . This is in great contrast to the measurements of the host of GRB 980703, which was found to have a SFR of  $\sim 500 M_\odot \text{ yr}^{-1}$  measured from its radio flux (Berger et al. 2001; Berger et al. 2003). The GRB 990712 host has an IR-luminosity which is 20 times less than that of the luminous GRB 980703 host. This suggests that different types of galaxies

can host GRBs some having more dust enshrouded star formation than others.

## 3. Imaging and photometry

We have analysed both ground based and HST images of the host of GRB 990712. The ground-based observations consist of *UBVRIJHKs* images obtained at different dates and using different instruments. All of the data presented here were obtained more than one year after the burst, so that the flux contribution from the afterglow is negligible. The data obtained from the Danish 1.5-m in September 2000 consist of images in Bessel *B*, *V* and *R* and Gunn *I* filters, and the *U* band data were obtained at the ESO 3.6-m telescope the night of Aug. 13, 2001 using the EFOSC2 instrument. Near-IR *JHKs* images were obtained at the NTT with the SOFI instrument over two nights from Aug. 1–2, 2001. Only the first night was photometric according to the ESO webpage<sup>1</sup>.

In order to obtain a more reliable optical estimate of the SFR of the host of GRB 990712, we performed spectroscopic observations centered on  $H\alpha$ , using FORS2 on the VLT.

The following sections describe the details of the data reduction, calibrations and combination of the different data sets.

### 3.1. HST/STIS images

The HST/STIS images of the host of GRB 990712 were obtained on April 24, 2000 as a part of a survey of GRB hosts (Fruchter et al. 2000b)<sup>2</sup>. The GRB hosts are observed through a clear (unfiltered) aperture (the 50CCD filter, which in the following analyses will be called the CL filter) and a long pass imaging filter, F28×50LP (called the LP filter).

The sensitivity of the CL filter extends from 4000 Å to 9000 Å, with its peak at  $\sim 5800$  Å, which falls within the *V* passband. The sensitivity of the LP filter extends from 5500 Å to 9000 Å, with its peak at  $\sim 6000$  Å. The total integration time of the GRB 990712 host was 4080 s in each filters.

The individual images are combined using DITHER II, a package which includes several tasks needed for combining dithered HST images. Fruchter & Hook (2002) describe the drizzling of WFPC2 images, and we adopt this process for the HST/STIS images. This method allows a higher resolution in the final images than in the original STIS images. In the drizzling of the STIS images of the hosts, the parameters `pixfrac=0.6` and `scale=0.5` were used. This gives an output pixel size of  $0'.0254 \text{ pixel}^{-1}$  in a  $2k \times 2k$  frame.

### 3.2. Ground-based optical images

The DFOSC data in the *B*, *V*, *R* and *I* filters consist of 11, 15, 15, and 59 frames having total integration times of 12900 s, 10800 s, 7600 s, and 39950 s, respectively. The individual integration times in each filter were not of equal length.

<sup>1</sup> <http://www.eso.org/gen-fac/pubs/astclim/forecast/meteo/CIRA/images/repository/lossam/>

<sup>2</sup> The FITS files of this and other hosts can be downloaded at [http://www.ifa.au.dk/~hst/grb\\_hosts/intro.html](http://www.ifa.au.dk/~hst/grb_hosts/intro.html)

The raw images were bias subtracted after inspection of the overscan region of the CCD. Any residual structure in the bias level was corrected for using a normalised median filtered bias image. The images were flat-fielded using flat fields obtained from a combination of several twilight sky observations. The selected flat fields produced reduced images in which the background signal varied by less than 2%, which is the limit for DFOSC data. The reduced images were WCS calibrated with a pipeline written by Andreas Jaunsen (ESO, Santiago). Approximately 50 reference stars from the USNO2 catalogue were used to compute the astrometry. From the WCS calibrated images, the shifts and rotations between individual images were found. The images were drizzled in much the same way as the HST images, not altering the pixel scale so the pixel size of the output image is  $0''.39 \text{ pixel}^{-1}$ .

The drizzling method was tested by comparing the final drizzled image with a median filtered image. The drizzling method gave a higher S/N for faint objects compared to the median combined image.

Another problem to take into account is the fringes that appear in the  $I$  band images and which depend on background level and consequently on the integration time. Although the fringes are large scale structures in the DFOSC images and should not introduce a large error when combining 59 individual images, they can be removed by construction of a fringe frame image. Such a frame is produced by replacing the pixel values of all stars with a small pixel value, while also replacing their neighboring pixels and combining the images using a threshold rejection. The resulting fringe image was scaled to the exposure time of each image and subtracted. This removed the fringes from the images in almost all cases. In a few ( $\sim 5$ ) images the background was higher, and the fringes were removed by subtracting a scaled fringe frame, with a scale factor higher than the integration times.

The photometric reference stars in the field were adopted from Sahu et al. (2000) and no re-calibrations of the field in the  $VRI$  bands were done. Some of the reference stars in Sahu et al. (2000) were saturated in the longest DFOSC  $V$ ,  $R$  and  $I$  band exposures so the shortest exposures were analysed in order to find secondary standard stars in the field which could be used as photometric reference stars in the combined frame. The magnitudes were derived by performing relative aperture photometry on the field with the PHOT package in IRAF. A section of a DFOSC image is shown in Fig. 1 where the stars denoted A, B, C, and D correspond to the standard stars in Sahu et al. (2000), while the numbers represent the secondary standard stars. The magnitudes are listed in Table 1.

For the  $B$  band, calibration images were taken in June 2001 using the Danish 1.5 m with DFOSC. The standard field PG 1657 from Landolt (1992) was observed 4 times during the photometric night. This field contains 4 standard stars. Only  $B$  band data were taken of the field containing the host of GRB 990712. The uncertainty of the  $B$  band calibration is 8% as estimated by standard procedures in IRAF. The errors are propagated in quadrature assuming that the errors are independent.

The  $U$  band data consist of  $4 \times 15$  min and one 10 min exposures. The images were reduced in the standard way and coad-

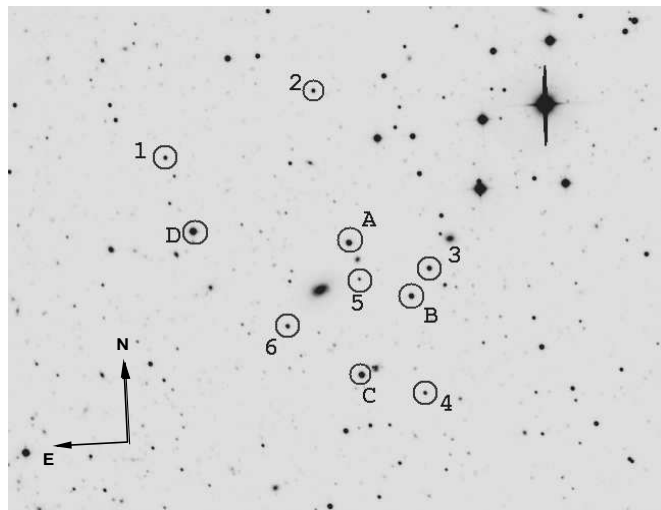


**Fig. 1.**  $I$  band field surrounding the GRB 990712 host. North is up and east is left as indicated, and the lengths of the arrows are  $1'$ . The stars denoted 1–6 are secondary reference stars, and the stars denoted A, B, C, and D correspond to the reference stars 1, 2, 3, and 4 in the paper of Sahu et al. (2000). The GRB host itself lies very close to the circle surrounding star A, and is not visible in the representation here. The magnitudes of the stars are listed in Table 1.

ded using the drizzle program without changing the pixel sizes. The night was photometric according to ESO's monitoring of the night sky conditions at La Silla. The zero point, extinction coefficient in the  $U$  band, and colour term of the night were given by Ramana M. Athreya (private communication). The  $U$  band magnitudes of the reference stars A, B, C, and D were measured in the 4 individual images, and the magnitude of the host was obtained using relative photometry in the coadded image using a  $2''.4$  radius aperture. This aperture was the same used for the DFOSC images. The resulting magnitudes of the host in all filters are given in Table 2. The photometric measurements were checked with SExtractor (Bertin & Arnouts 1996), and with aperture photometry we found magnitudes consistent with those in the Table within  $1\sigma$  errors.

### 3.3. Ground-based near-IR images

For the reduction of the near-IR  $JHKs$  SOFI data, a sky image was constructed from 6–10 object images obtained immediately before and after each frame. The number of images depends on the quality of the sky subtraction which was evaluated by eye. The sky subtracted images were divided by a flat field obtained from the NTT/SOFI webpages. A flatfield multiplied with an illumination corrected image shows variations on the order of 0.2% during a month, and the reduction described here gave flatfield accuracies of 1%.

The integration times were  $31 \times 15$  s,  $40 \times 15$  s, and  $20 \times 15$  s for the  $H$ ,  $Ks$ , and  $J$  band respectively. The exposures were divided into two sets, one for each day, which were reduced separately. Standard star observations were done right after the science exposures. The extinction coefficients were adopted from the NTT/SOFI webpages. The corrections for atmospheric extinction are small, because the standard star observations were

Std.	<i>U</i>	<i>B</i>	<i>V</i>	<i>R</i>	<i>I</i>	<i>J</i>	<i>H</i>	<i>Ks</i>
1	–	–	19.84±0.02	18.76±0.02	17.48±0.03	–	–	–
2	19.16±0.07	–	18.21±0.01	17.87±0.02	17.48±0.03	–	–	–
3	–	–	19.08±0.02	17.94±0.02	16.57±0.03	–	–	–
4	–	–	18.90±0.02	18.37±0.02	17.86±0.03	–	–	–
5	–	–	20.72±0.04	19.73±0.02	18.68±0.04	–	–	–
6	–	–	19.21±0.01	18.31±0.02	17.34±0.03	–	–	–
A	18.80±0.06	18.80±0.06	17.16±0.01	16.40±0.01	15.64±0.01	14.82 ± 0.02	14.20 ± 0.03	14.04 ± 0.04
B	–	17.91±0.05	16.98±0.01	16.65±0.01	16.29±0.01	15.91 ± 0.02	15.60 ± 0.04	15.57 ± 0.03
C	–	17.69±0.07	16.46±0.01	15.97±0.01	15.50±0.01	14.96 ± 0.02	14.51 ± 0.04	14.42 ± 0.04
D	17.69±0.07	17.33±0.06	15.91±0.01	15.27±0.01	14.65±0.01	13.99 ± 0.02	13.39 ± 0.03	13.28 ± 0.03

**Table 1.** Magnitudes of the secondary standard stars. The “–” signs appear where the magnitudes for the stars have not been derived either because they were saturated in some images, which was the case of the B and C stars, or they were faint and therefore gave large photometric errors ( $> 0.08$ ). These were disregarded in the case of the *U*, *B*, and near-IR bands of the secondary standards 1–6. The *VRI* band magnitudes of A, B, C, and D are taken from Sahu et al. (2000).

performed at an airmass different by only 0.1 from the science observations. Likewise, the colour terms in the near-IR are small ( $\lesssim 0.02$ ). The images of the standard star were analysed in order to find the zero point in each filter. The transformation equations did not include a colour term, as this produced uncertain fits, are given by:  $J_{\text{inst}} = j1 + J_{\text{std}}$ , where  $J_{\text{inst}}$  is the instrumental magnitude and  $J_{\text{std}}$  is the standard magnitude. The transformations for the *H* and *Ks* data are similar. The fitted zero points are:  $j1 = 23.06 \pm 0.005$ ,  $h1 = 22.937 \pm 0.003$  and  $k1 = 22.367 \pm 0.004$ . These zero points agree with the values posted on the NTT/SOFI webpages.

The shifts between the reduced images were found using `precor`, `crossdrizz` and `shiftfind`, and the images in each field were combined using `imcombine`. The images were combined using a common median zero-point background value, and applying a bad-pixel mask obtained from the SOFI webpages to reject hot or dead pixels in the combination.

The magnitudes of the reference stars (the same 4 stars as in Sahu et al. (2000)) were measured in 10 individual frames for each filter, and the magnitude of the host was found by performing relative photometry to the 4 stars in the co-added images. The magnitudes of the reference stars are presented in Table 1, and the near-IR magnitudes of the host are given in Table 2 which also presents the fluxes in the various bands. The fluxes are obtained by correcting the magnitudes for the Galactic reddening  $E_{B-V} = 0.033$  estimated from the dust maps of Schlegel et al. (1998). Then the magnitudes are converted to AB magnitudes. Due to the faintness of the host in the near-IR, the errors are dominated by sky noise.

The near-IR magnitudes were obtained using the flux enclosed within a circular radial aperture of  $1''.2$ . At optical wavelengths, the flux of the host is not contained within this aperture due to worse seeing. In order to get the right colour of the host, an offset equal to the difference in the *I* band magnitude between an aperture of  $1''.2$  and  $2''.4$  was added. This will then provide the right  $I - J$  colour, as well as a smaller photometric error. The same method was applied for the *H* and *Ks* data. As long as the colour gradient in the host is negligible, this does not change the near-IR magnitudes one would have calculated from larger apertures. The colour gradient of the host is negli-

filter	magnitude	flux ( $\mu\text{Jy}$ )
<i>U</i>	23.12±0.05	1.00±0.05
<i>B</i>	23.36±0.09	2.00±0.06
<i>V</i>	22.39±0.03	4.43±0.16
<i>R</i>	21.84±0.02	6.31±0.20
<i>I</i>	21.41±0.03	7.01±0.29
<i>J</i>	20.81±0.17	7.68±1.21
<i>H</i>	20.25±0.19	8.22±1.47
<i>Ks</i>	19.98±0.28	6.74±1.71

**Table 2.** Magnitudes and corresponding fluxes of the host of GRB 990712 from all ground based observations. The fluxes in column 3 are obtained by correcting for a Galactic reddening of  $E_{B-V} = 0.033$ , and offsetting to the AB system before converting the magnitudes to fluxes. The flux errors do not include the uncertainty of the Galactic reddening. The *R* band magnitude is consistent with that derived in Hjorth et al. (2000).

ble at a radius larger than  $1''$  estimated from the morphological study of the HST images described in detail in Section 5. We find that there are colour gradients in the central  $0''.25$ , but this has no impact on radii larger than  $1''.2$ . The *K* band magnitude is consistent with the value reported in Le Floch et al. (2003).

## 4. Spectroscopy

The host galaxy of GRB 990712 was observed in service mode with FORS2 at UT4 of ESO’s Very Large Telescope on July 18, 2001. The exposure time was 10 min, and the grism used was GRIS 600z+23 with order separation filter OG590, giving a wavelength range of 7400–10700 Å, which includes the redshifted wavelength of the host galaxy’s  $H\alpha$  at 9404 Å. The slit width was set to  $1''$ , resulting in a resolving power of approximately 1400. The seeing during the observations was around  $0''.8$ . The spectrum was reduced in the standard fashion, using IRAF. The wavelength calibration was performed using a HeNeAr lamp spectrum; the resulting scatter is  $0.02$  Å.

The resulting spectrum has a bright  $H\alpha$  emission line at 9404 Å which has an observed equivalent width (EW) of  $180 \pm 40$  Å estimated from fitting the continuum level by spline

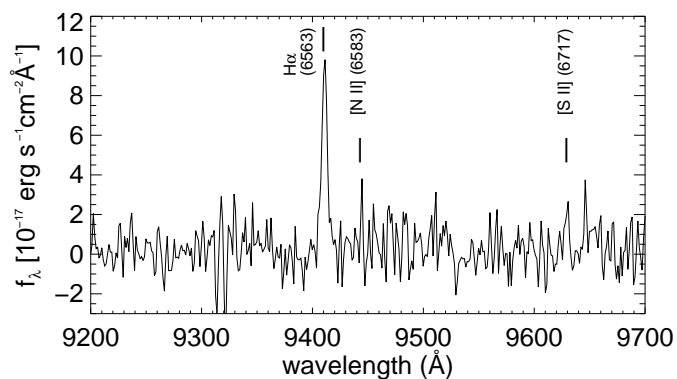


**Fig. 2.** Section of the spectrum containing the redshifted  $H\alpha$  line. The spectrum has been wavelength calibrated, and set to a flux scale corresponding to the continuum level of  $7.38 \mu\text{Jy}$  estimated from the SED analysis. The redshift measured from the  $H\alpha$  line is 0.4331. At  $9436.4 \text{ \AA}$  a faint emission line from  $[\text{N II}] \lambda 6583$  is present, corresponding to  $z = 0.4338$  after applying a standard air to vacuum correction, and at  $9621 \text{ \AA}$  a line from  $[\text{S II}] \lambda 6717$  corresponding to  $z = 0.4328$  can be seen.

polynomials of different orders. A small part of the spectrum is shown in Fig. 2. One clearly sees the  $H\alpha$  line and also at low  $S/N$  levels, the  $[\text{N II}] \lambda 6583$  line and the  $[\text{S II}] \lambda 6717$ . The measured EW of the  $H\alpha$  line indicates that the host is a young star-forming galaxy. The starburst99 models provide a relation between the rest frame  $H\alpha$  EW and the age of a stellar population (Leitherer et al. 1999). With a rest frame EW of  $125 \pm 28 \text{ \AA}$  one would expect an instantaneous starburst age of  $\sim 6 \text{ Myr}$  according to the Starburst99 models, assuming solar metallicity. A lower metallicity of  $Z = 0.001$  would increase this age estimate by a factor of 2. Furthermore, the EW of  $H\beta$  reported in Vreeswijk et al. (2001a) supports a starburst age of  $\sim 6 \text{ Myr}$  according to the Starburst99 models. In the case of a continuous star formation rate of  $1 M_{\odot} \text{ yr}^{-1}$  the inferred age from the EW is  $\sim 60 \text{ Myr}$ , i.e. in both scenarios the presence of a young population is inferred.

## 5. Morphology of the host galaxy

In the HST images the size of the GRB host is  $1''.3 \times 0''.9$ . The STIS images have revealed that the host of GRB 990712 has two separate intensity peaks, and neither of these are located at the geometrical center of the host. An image and a contour plot of the host is shown in Fig. 3. The rightmost knot (south-east=SE) is  $\sim 1 \text{ mag}$  brighter than the left (north-west=NW). The GRB occurred in the SE knot within  $0''.048 \pm 0''.080$  of the center. The afterglow itself will not contribute significantly to the flux of the host if a break in the light curve is present around one day after the burst as suggested in Björnsson et al. (2001). If no such break occurred, the contamination of the SE knot due to the late time afterglow will be  $\sim 5\%$ . If a supernova of similar brightness as SN 1998bw is present at the time of the observations, it would have the magnitude  $V \approx 27.0$  at  $z = 0.433$ . This magnitude is calculated assuming a similar late time supernova light curve contributing to the total flux in addition to

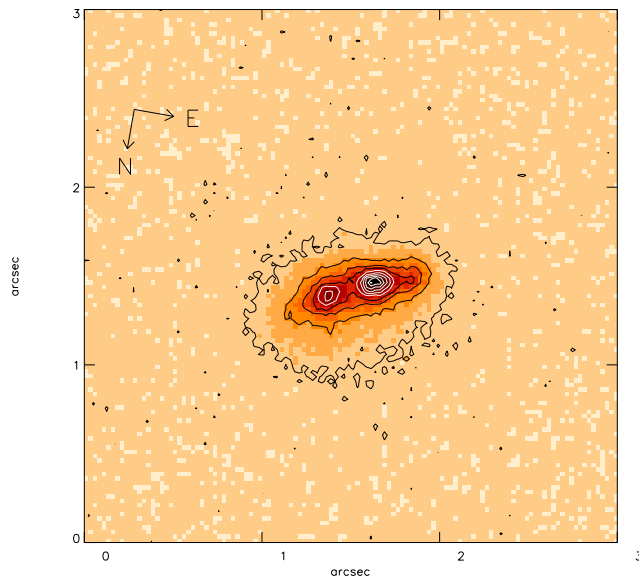


**Fig. 3.** A STIS CL image of the host of GRB 990712 overlaid by a contour plot shows that there are two intensity peaks in the image. The scale of the plot is  $3'' \times 3''$ . The distance between the two peaks is 10 drizzled pixels, or  $0''.25$ , which corresponds to a separation of  $\sim 1500 \text{ pc}$  at  $z = 0.433$ . At the time of observation more than one year from the burst the flux contribution from the afterglow will be negligible.

the afterglow. If a SN is present, the contamination of the SE knot will be an additional  $\sim 5\%$ .

The colours of the two knots were analysed by performing aperture photometry centered on each knot using both the CL and LP images. At a redshift of  $z = 0.433$  the difference in magnitudes in these filters roughly corresponds to the rest-frame  $B - V$  colour. The  $B - V$  colour of the NW knot is  $1.3 \pm 0.1$ , and the colour of the SE knot is  $0.9 \pm 0.1$  within an aperture of radius  $0''.076$  (i.e. 3 drizzled pixels). The colour becomes more red with increasingly larger photometric apertures (up to  $0''.15$  radius, i.e. 6 drizzled pixels), but the colour gradient in the NW knot is smaller than in the SE knot. At larger apertures, the colours will be contaminated by flux from the other knot. The differences in colour could be caused by different ages of two starburst regions, the bright blue knot being slightly younger than the fainter. Another explanation could be a relatively larger extinction in the NW knot. If the colour excess,  $E_{B-V}$ , of the faint knot is larger than 0.34 than for the bright knot, this could explain the colour difference. Compared to the overall extinction estimated from the SED this is relatively large. Even though we find no evidence for a large extinction from the SED analysis as explained in Section 6, the morphology of the host supports the presence of two different stellar components.

Most interestingly, the GRB was coincident with the center of the blue SE knot (Bloom et al. 2002b). This location of the GRB corresponds to the bluest part of the host, which likely links the GRB to a star-forming site. If the two knots were the

result of a merging of two components, then one would expect to see further evidence of the tidal interaction in, for example, luminous tails. This is not apparent in the image, but for low mass systems bright tails are probably rare. One should note that the surface brightness of tidal tails can be low and thus difficult to detect, since the redshift of the host gives a further factor  $(1+z)^4$  dimming of the surface brightness assuming a standard cosmology.

## 6. Spectral energy distribution of the host

The magnitudes in Table 2 were used to compare to theoretical galaxy template spectra from Bruzual & Charlot (1993). This was done by the program HyperZ<sup>3</sup> described in Bolzonella et al. (2000). HyperZ was written mainly for obtaining the photometric redshifts of galaxies in large surveys, but it also serves the purpose for finding the best matching theoretical galaxy template for a given set of broad band observations. The templates consist of elliptical, several types of spiral, irregular, and starburst spectra at various ages having different star formation histories. The time evolution is described by  $SFR \propto \exp(-t/\tau)$ , where  $\tau$  is the SFR timescale which increases along the Hubble sequence, with  $\tau \rightarrow 0$  in the case of an instantaneous starburst. The metallicities of the templates are equal to the solar value,  $Z=0.02$ . Gorosabel et al. (2003a,b) have shown that for the GRB 000210 and GRB 000418 hosts, the metallicity is a secondary variable in comparison to the impact of the assumed IMF and the extinction law.

We used both the Miller & Scalo (1979) initial mass function (IMF) and the Salpeter (1955) IMF for stellar masses between 0.1 and 125  $M_{\odot}$  for calculating the templates. The Miller & Scalo IMF produces fewer massive stars compared to a Salpeter IMF, and at masses below 1  $M_{\odot}$  the Miller & Scalo IMF is flatter (Miller & Scalo 1979). The largest differences between the templates are at the red and near-IR wavelengths. Different amounts of internal extinction can also be applied to the templates. In this way, the SED fitting allows an estimate of the type of galaxy, age, and internal extinction. In the analysis the redshift of the templates was fixed to the value of the host ( $z = 0.433$ ). Leaving the photometric redshift  $z_{\text{phot}}$  as a free variable gives  $z_{\text{phot}} = 0.445 \pm 0.020$ , which is consistent with the spectroscopic one. This additional free parameter does not change any of the resulting values from the best fit besides changing the reduced  $\chi^2$  by a small amount. The agreement between the photometric and the spectroscopic redshift shows that the SED fitting technique is reliable for estimating other properties of the host.

The goodness of the fit is evaluated by the expression:

$$\chi^2 = \sum_i \left( \frac{F_{\text{host},i} - k \times F_{\text{temp},i}}{\sigma(F_{\text{host},i})} \right)^2 \quad (1)$$

where the sum is to be taken over all filters,  $i$ . The flux values of  $F_{\text{host}}$  are found in Table 2,  $\sigma(F_{\text{host},i})$  is the photometric error, and  $k$  is a normalization constant.  $F_{\text{temp},i}$  is the flux of the template in the filter  $i$ , which is calculated using the throughput for the given filter and instrument. For the DFOSC and

EFOSC data, the filter transmission was convolved with the quantum efficiency of an ESO LORAL CCD in order to calculate the throughput. For the NTT data, the combined throughput of SOFI and the filters were used.

The SED of the host was best fit by a starburst template. This confirms the conclusion in Vreeswijk et al. (2001a), derived on the basis of emission lines, that the host is a starburst galaxy. The best fit model has a starburst age of 0.255 Gyr and an extinction of  $A_V = 0.15 \pm 0.1$  using a Salpeter IMF for the templates. The error in the extinction was estimated from results of the fits for which the  $\chi^2$  per degree of freedom,  $\chi^2/\text{dof} < 2$ , and all these fits gave an age of 0.255 Gyr. Fig. 4 shows the best fits when using templates from a Miller & Scalo IMF (thin line) and a Salpeter IMF (thick line) respectively. Both templates gave the same values for the extinction and age for the best fit. The fit to the thin line has a reduced  $\chi^2/\text{dof} = 2.82$  and a fit to the thick line has  $\chi^2/\text{dof} = 0.959$ . The largest difference between the two templates is in the near-IR, where our photometric points have large uncertainties.

Fitting the SED to other types of galaxy spectra give larger values of  $\chi^2$ , e.g.  $\chi^2/\text{dof} = 14.3$  for the best fit to an irregular galaxy template, and  $\chi^2/\text{dof} = 16.2$  to an elliptical galaxy. For the latter template, all the measured near-IR fluxes were  $\sim 3\sigma$  below the template flux. Generally, all other templates besides starburst templates fail to reproduce the flat continuum from 8000–22000 Å, while at the same time fitting the Balmer jump at the rest-frame 3646 Å. Thus, we infer that the host is most likely a starburst galaxy with a stellar distribution similar to a Salpeter IMF.

The precision of the age estimation relies upon the accuracy of how well the Balmer jump is sampled. At the redshift of the host, this jump will lie at  $\sim 5200$  Å. It is seen in Fig. 4 that with the current set of broad band magnitudes this jump is well sampled. Therefore, the age of the dominant population of stars is well constrained. However, if more than one population of stars is present in the host, this will change the age determination somewhat as explained in section 6.1.

The extinction found by HyperZ is  $A_V = 0.15$  using the extinction curve from Calzetti et al. (2000) appropriate for starburst galaxies. The extinction measured from emission line widths was  $A_V = 3.4^{+2.4}_{-1.7}$ , which is consistent with a small extinction measured from the SED. We also tried to do the SED fitting with other extinction curves. The  $A_V$  found by HyperZ was found not to vary much ( $A_V \lesssim 0.2$  in all cases) using the extinction curve of the Milky Way (MW) from Seaton (1979), the Large Magellanic Cloud (LMC) from Fitzpatrick (1986), and the Small Magellanic Cloud (SMC) from Prevot et al. (1984) respectively. Acceptable values of  $\chi^2/\text{dof} < 1.5$  for the fits were found using the starburst, LMC, and SMC extinction curves, so the extinction curve could not be constrained from the SED. A larger  $\chi^2/\text{dof} = 2.2$  was produced using a MW extinction curve, which suggests that the dust in the host is different than from MW dust. This is in agreement with results obtained from other GRBs, where the extinction law has been inferred from studying the afterglows. Jensen et al. (2001), Fynbo et al. (2001), Lee et al. (2001), and Holland et al. (2003) find that the SMC extinction law gives a better fit to multiband ob-

<sup>3</sup> <http://webast.ast.obs-mip.fr/hyperz/>

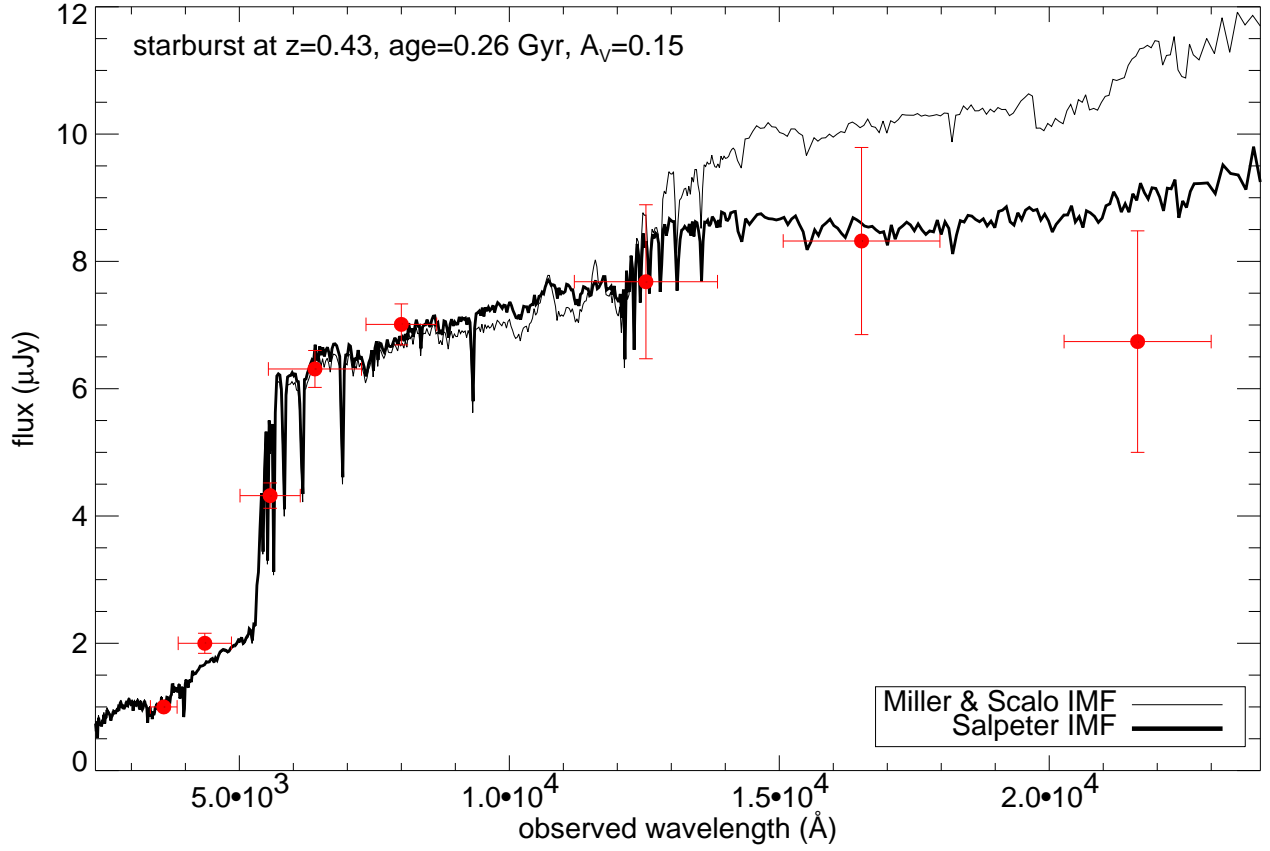


**Fig. 4.** Best fit of the GRB host SED to synthetic spectra calculated by the HyperZ program. The synthetic spectra are shown by the two solid lines and the dots denote the *UBVRIJHKs* fluxes from Table 2. The horizontal errorbars indicate the FWHM of each filter. The thin line shows a template spectrum calculated using a Miller & Scalo IMF while the thick line is calculated using a Salpeter IMF. The values of the photometric redshift, age, and extinction are given as inserts in the panel. A starburst extinction curve is used for the calculation of the extinction.

servations of the afterglows of GRB 000301C, GRB 000926, GRB 010222, and GRB 021004, respectively.

From the SED of the host we can determine the absolute magnitude in various bands by convolving the restframe spectrum of the best fitting template with various filter transmission curves. This gives  $M_B = -18.8$ ,  $M_V = -19.9$ , and  $M_R = -20.3$  in the assumed cosmology, corrected for Galactic extinction. This absolute magnitude is comparable to that of other hosts (Bloom et al. 1998, 2001; Sokolov et al. 2001). The luminosity of the galaxy is less than the characteristic luminosity  $L^*$  given by the Schechter function. For field galaxies a value of  $M_B^* = -21$  is typically assumed, while for starburst galaxies at high redshift this magnitude is highly uncertain, but is likely to be brighter than  $-21$  (Lilly et al. 1995). GRB hosts have been shown typically to be under-luminous (Le Floc'h et al. 2003). From the early optical light curves of the optical transient, obtained in the *V*, *R*, and *I* bands when it was still bright, Sahu et al. (2000) estimated the luminosity of the underlying host to be of the order of  $L^*$ . Using high spatial resolution HST images Hjorth et al. (2000) refined the luminosity of the galaxy to be  $0.2L^*$ .

### 6.1. Two population fits

The scenario described above, where the whole spectrum of the galaxy can be represented by one single burst of star formation is likely too simple. One must expect that more than one burst of star formation would contribute to the total mix of stars observed. With the knowledge that some GRBs originate from collapsing massive stars, we would expect a population of younger stars to be present, which is supported by the large EW of the  $H\alpha$  line. We therefore investigated whether the SED of the host could be explained by a superposition of two populations of stars, i.e. a young burst superimposed onto an older population.

The method applied was as follows. We created two new SEDs, a red and a blue one, whose sum was the total SED of the observed galaxy. The two objects were run through HyperZ, finding the best fit templates using the same templates as in the single population case. The best fit spectra of the two populations were summed and compared to the broad band fluxes of the host, and the  $\chi^2$ s of the fits were calculated using Eq. (1). It was then investigated by iterations if a bluer first population plus a redder second population would produce a better fit to the observations.



This process was done first with two populations of similar total flux. In a second run, the observed flux was partitioned into 80% for the first population and 20% for the second.

We found that several two population models were able to fit the observations with  $\chi^2/\text{dof} \approx 1$ . As shown in the upper panel in Fig. 5, the total flux can originate from two rather similar instantaneous burst populations. In this specific case, one of the populations has an age of 0.36 Gyr and an extinction of  $A_V = 0.12$ , while the other has an age of 0.18 Gyr and zero extinction. The fit of the summed spectrum to the observations is  $\chi^2/\text{dof} = 0.66$ .

Another scenario could also explain the properties of the host. The lower panel in Fig. 5 shows the result of the first population of stars being a 0.36 Gyr old starburst, while the flatter spectrum corresponds to a less luminous second population, which is a 52 Myr starburst. Both these spectral templates have  $A_V = 0.00$ . The fit of the summed spectra to the observations gives  $\chi^2/\text{dof} = 0.75$ . We therefore conclude that if a second population of stars has a significant contribution to the total flux, the age will be 50–200 Myr, found from acceptable values of the  $\chi^2/\text{dof}$  fits. Considering the large observed  $H\alpha$  EW we find that a young population ( $\sim 50$  Myr) is preferable. Even younger ages for the second population can not be ruled out. By constructing templates of very young populations of stars, we can estimate the total flux allowed from such a population. The constraining factor is the weak blue continuum observed. If a stellar population with an age of 10 Myr is present, the total (bolometric) flux it emits is less than 5% of the total observed flux from the host.

## 7. Star-formation rate

The continuum in the UV part of the spectrum (1500–2800 Å) mainly comes from young OB stars, and a relation between the UV flux and the SFR can be derived by comparison of observed spectra to synthetic model spectra (K98).

We interpolate between the observed flux in the  $U$  and the  $B$  band, and the flux at the wavelength  $2800(1+z)$  Å is estimated assuming a powerlaw spectrum,  $F_{\text{host}} \propto \nu^\beta$ . We do not consider any best template fit for the calculation of the flux at this wavelength. The total luminosity at  $2800(1+z)$  Å can be calculated given the cosmological model, and converted to an overall SFR of the host. K98 gives the relation between the UV luminosity and the SFR for a Salpeter IMF.

$$\text{SFR} (M_\odot \text{ yr}^{-1}) = 1.4 \times 10^{-28} \times L_{\nu, \text{UV}} \quad [\text{erg s}^{-1} \text{ Hz}^{-1}] \quad (2)$$

This expression is adequate for galaxies with constant stellar formation over time scales of at least  $10^8$  years. The coefficient that links the SFR with the UV luminosity ( $1.4 \times 10^{-28}$  in the case of Eq. (2)) is significantly lower in younger stellar populations present in starburst regions. Thus, this SFR has to be considered as an upper limit. However, in starburst regions dust is expected to be present, and a correction for dust extinction is necessary in order to find the UV flux. We have in the SED analysis found only a small global extinction effect, but it could be locally higher if the medium is clumpy. For instance, the appreciable extinction inferred along the line

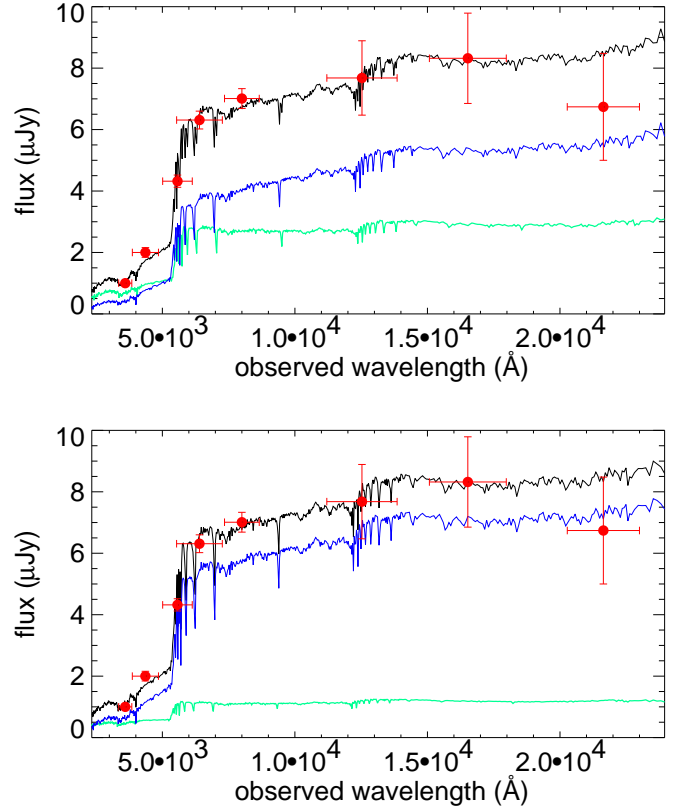


**Fig. 5.** Two examples of the best fits for two populations. In both panels the best fit spectra for each of the components are shown along with the summed spectrum. In the upper panel, the lower spectrum corresponds to a 0.18 Gyr starburst population, the middle spectrum to a 0.36 Gyr starburst population, and the upper spectrum to a sum of the two. The fit has  $\chi^2/\text{dof} = 0.66$ . In the lower panel, the lower spectrum corresponds to a 52 Myr starburst population, and again the upper spectrum to a sum of the two. This fit has  $\chi^2/\text{dof} = 0.75$ .

of sight to some afterglows derived from the curvature of the near-IR/optical afterglow SEDs in e.g. GRB 000301C in Jensen et al. (2001), and GRB 000926 in Fynbo et al. (2001) seem to indicate that GRB progenitors tend to be embedded in dusty local regions. High  $N_H$  values derived from X-ray afterglow spectra also supports this scenario (Piro et al. 2002). This will lead to an underestimate of the local extinction, and hence of the SFR. This opposite effect may mitigate the SFR overestimation entailed in Eq. (2). The estimated SFR value has to be considered as the sum of the SFR contributions coming from the two potential stellar populations.

We calculate a flux at the rest frame 2800 Å of  $1.65 \pm 0.04$   $\mu\text{Jy}$  which translates into a SFR of  $1.3 \pm 0.3 M_\odot \text{ yr}^{-1}$ , which is similar to the SFR of a galaxy such as the Milky Way. The errors due to the flux measurements and interpolation between the two bands are insignificant compared to the uncertainty of the conversion factor, which is  $\sim 30\%$ . Correcting for the extinction of  $A_V = 0.15$  using the starburst extinction curve from Calzetti et al. (2000) gives a slightly larger flux at 2800 Å in the rest frame, and the SFR is a bit larger:  $1.6 \pm 0.3 M_\odot \text{ yr}^{-1}$ .



We also estimate the SFR from the  $H\alpha$  line flux. K98 gives the relation between the  $H\alpha$  luminosity and the SFR:

$$\text{SFR} (M_{\odot} \text{ yr}^{-1}) = 7.9 \times 10^{-42} \times L_{H\alpha} \quad [\text{erg s}^{-1}] \quad (3)$$

We can find the line flux,  $f_{\text{line}}$ , and the luminosity,  $l_{\text{line}}$ , once the continuum flux  $f_{\text{cont}}$  at the wavelength of the redshifted  $H\alpha$  line  $\lambda$ , and the equivalent width  $EW$  is known.

$$\begin{aligned} f_{\text{line}} &= f_{\text{cont}} \times c/\lambda^2 \times 10^{-10} \times EW \\ l_{\text{line}} &= f_{\text{line}} 4\pi d_L^2 \end{aligned} \quad (4)$$

Since the spectrum has not been flux calibrated, we estimate the continuum level by interpolation between the  $I$  and  $J$  band fluxes assuming a powerlaw spectrum. We find a continuum level of  $(7.38 \pm 0.44) \mu\text{Jy}$ . Using Eq. (4) we find  $f_{\text{line}} = (4.50 \pm 1.00) \times 10^{-16} \text{ erg s}^{-1} \text{ cm}^{-2}$ , which gives a  $\text{SFR} = (2.8 \pm 0.7) M_{\odot} \text{ yr}^{-1}$ . The error includes the uncertainty of the conversion from flux to SFR, which is 30%. The two calculated SFRs are consistent with each other within  $2\sigma$ .

The larger SFR inferred from the  $H\alpha$  line compared to the SFR found from the UV flux could be due to dust extinction, which is stronger in the UV region. The ratio between the  $H\alpha$  line flux and the  $H\beta$  line flux,  $(1.33 \pm 0.20) \times 10^{-16} \text{ erg cm}^{-2} \text{ s}^{-1}$  in Vreeswijk et al. (2001a), is  $3.38 \pm 0.90$ , while the expected ratio in H II regions in the case of no extinction is 2.85 (Osterbrock 1989). The ratio between the observed line fluxes thus corresponds to a magnitude difference of  $0.19 \pm 0.31$ . Using the extinction curve from Calzetti et al. (2000) an extinction of  $A_V = 0.60 \pm 0.99$  is inferred from the line ratio. The calculated extinction is the same when using the MW extinction curve from Fitzpatrick (1999), while in the case of an SMC extinction curve one would find  $A_V = 0.41 \pm 0.60$ . The extinction is therefore consistent with the small value indicated by the SED analysis.

The SFR of this host is in the same range as the SFRs found for other hosts through their rest frame UV flux, which typically gives SFRs  $< 10 M_{\odot} \text{ yr}^{-1}$  (Fruchter et al. 1999; Bloom et al. 1998; Djorgovski et al. 2001). The largest SFRs found from optical methods to date are  $20 M_{\odot} \text{ yr}^{-1}$  for the GRB 990703 host (Djorgovski et al. 1998) and  $55 M_{\odot} \text{ yr}^{-1}$  for the GRB 000418 host (Bloom et al. 2002a), although a smaller SFR based on the UV region of the latter host has been inferred (Gorosabel et al. 2003b). It must be pointed out that these SFRs are strictly lower limits to the true SFRs since the reported values are not corrected for extinction by dust in the hosts. Radio and sub-mm data suggest SFRs one or two orders of magnitude larger than the optical inferred SFRs for a sample of GRB hosts (Berger et al. 2003).

## 8. Discussion and conclusions

From broad band magnitudes in  $UBVRIZJK_s$  filters we have examined the SED of the host of GRB 990712. Comparing this SED with model templates of different galaxy types, we found that the host is a starburst galaxy with an extinction of  $A_V = 0.15$ . With spectroscopic observation of the host we

calculated the extinction  $A_V = 0.6 \pm 0.99$  from the  $H\alpha/H\beta$  line ratio, confirming a small extinction value.

In the collapsar scenario the progenitor of the GRB may be embedded in a molecular cloud having a much larger extinction due to the surrounding dust. Thus, even though we can estimate the overall internal extinction in the host in the particular case of GRB 990712, it is not possible to say anything about the extinction in the line of sight towards the burst itself. It could well be much higher. However, analyses of several afterglows have failed to reveal a very high extinction ( $A_V > 1$ ). According to Galama & Wijers (2001), the expected visual extinction of the afterglows should be much higher when compared to the column density inferred from the X-ray afterglows of several bursts. They argued that dust can be destroyed along the line of sight towards the burst making the visual extinction appear smaller. Waxman & Draine (2000) have calculated that dust can be destroyed out to a distance of 10 pc from the burst site. The extinction inferred from the SED fitting is an overall average extinction of the entire galaxy. Therefore it is necessary to investigate further the relation between the small extinction inferred from the optical light curves of some GRBs,  $A_V < 0.2$  (Andersen et al. 2000; Galama & Wijers 2001; Jensen et al. 2001; Fynbo et al. 2001; Stanek et al. 2001), and the extinction in the host itself.

The SED of the host is similar to that of a starburst population with an age of 0.26 Gyr at a redshift of 0.43. This age is still consistent with a merging neutron star scenario as the progenitor of the GRB. It is now known that some of the long-duration GRBs are associated with collapsing massive stars (Stanek et al. 2003; Hjorth et al. 2003). Considering that the life times of the most massive stars are of the order of a few Myr, a small age of the star burst is expected. It was therefore investigated whether two distinct populations were able to fit the broad band observations of the host. It was found that in such case, the best fits were produced by a younger starburst population with an age of 50–180 Myr, and zero extinction. We consider the lower limit to be more likely given the large  $H\alpha$  EW found in the spectrum, which suggests presence of a young stellar population with an age of 6–60 Myr depending on the star formation history.

From the analysis of the SED we found that a Salpeter IMF was able to reproduce galaxy spectral templates corresponding to the observed fluxes.

We calculate the SFR by estimating the rest frame flux at 2800 Å. The  $\text{SFR} = 1.3 \pm 0.30 M_{\odot} \text{ yr}^{-1}$  is not very large, and correcting for internal extinction in the host does not increase the SFR much. This relatively small SFR is comparable to that of other GRB hosts found from using the same UV–SFR estimator. Considering that the host is less luminous than an  $M^*$  galaxy, this SFR is relatively high compared to present day galaxies. As the host is a  $0.2L^*$  galaxy we find a SFR per  $L/L^*$  of  $\sim 5 M_{\odot} \text{ yr}^{-1} (L/L^*)^{-1}$ .

Comparison with the SFR of  $2.8 \pm 0.7 M_{\odot} \text{ yr}^{-1}$  found from the  $H\alpha$  line flux implies that there may be moderate extinction present in the host. The dust may be distributed in a clumpy medium, where most of the UV flux is absorbed.

The analysis of the morphology of the host showed that it has two knots of different colours. This colour difference could

be due to two bursts of star formation. This interpretation is consistent with the large Balmer break in the SED which suggests the presence of an older population together with the large H $\alpha$  EW suggesting the presence of a very young population of stars.

Most importantly, the location of the burst was in the bluest part of the host galaxy, which supports the recent observations that the long-duration GRBs are linked to sites of formation of massive stars.

*Acknowledgements.* The observations from the Danish 1.5m Telescope were supported by the Danish Natural Science Research Council through its Center for Ground Based Observational Astronomy (IJAF). This work was supported by the Danish Natural Science Research Council (SNF). J. Gorosabel acknowledges the receipt of a Marie Curie Research Grant from the European Commission. We are grateful for the availability of the WCS pipelines provided by Andreas Jaunsen. Many thanks to Jeremy Bailin (Steward Observatory, University of Arizona) for useful comments on the paper.

## References

- Andersen, M. I., Hjorth, J., Pedersen, H., et al. 2000, *A&A*, 364, L54
- Bakos, G., Sahu, K., Menzies, J., Vreeswijk, P., & Frontera, F. 1999, *GRB Circular Network*, 387
- Berger, E., Cowie, L. L., Kulkarni, S. R., et al. 2003, *ApJ*, 588, 99
- Berger, E., Kulkarni, S. R., & Frail, D. A. 2001, *ApJ*, 560, 652
- Bertin, E. & Arnouts, S. 1996, *A&AS*, 117, 393
- Björnsson, G., Hjorth, J., Jakobsson, P., Christensen, L., & Holland, S. 2001, *ApJ*, 552, L121
- Bloom, J., Berger, E., Kulkarni, S., Djorgovski, G., & Frail, D. 2002a, *AJ*, in press
- Bloom, J. S., Djorgovski, S. G., & Kulkarni, S. R. 2001, *ApJ*, 554, 678
- Bloom, J. S., Djorgovski, S. G., Kulkarni, S. R., & Frail, D. A. 1998, *ApJ*, 507, L25
- Bloom, J. S., Kulkarni, S. R., & Djorgovski, S. G. 2002b, *AJ*, 123, 1111
- Bolzonella, M., Miralles, J.-M., & Pelló, R. 2000, *A&A*, 363, 476
- Bruzual, A. G. & Charlot, S. 1993, *ApJ*, 405, 538
- Calzetti, D., Armus, L., Bohlin, R. C., et al. 2000, *ApJ*, 533, 682
- Djorgovski, S. G., Frail, D. A., Kulkarni, S. R., et al. 2001, *ApJ*, 562, 654
- Djorgovski, S. G., Kulkarni, S. R., Bloom, J. S., et al. 1998, *ApJ*, 508, L17
- Eichler, D., Livio, M., Piran, T., & Schramm, D. N. 1989, *Nature*, 340, 126
- Fitzpatrick, E. L. 1986, *AJ*, 92, 1068
- . 1999, *PASP*, 111, 63
- Frontera, F. 1999, *GRB Circular Network*, 385
- Fruchter, A., Vreeswijk, P., Hook, R., & Pian, E. 2000b, *GRB Circular Network*, 752
- Fruchter, A. S. & Hook, R. N. 2002, *PASP*, 114, 144
- Fruchter, A. S., Pian, E., Gibbons, R., et al. 2000, *ApJ*, 545, 664
- Fruchter, A. S., Pian, E., Thorsett, S. E., et al. 1999, *ApJ*, 516, 683
- Fynbo, J. U., Gorosabel, J., Dall, T. H., et al. 2001, *A&A*, 373, 796
- Galama, T., Vreeswijk, P., Rol, E., et al. 1999, *GCN* 388
- Galama, T. J., Vreeswijk, P. M., van Paradijs, J., et al. 1998, *Nature*, 395, 670
- Galama, T. J. & Wijers, R. A. M. J. 2001, *ApJL*, 549, L209
- Gorosabel, J., Christensen, L., Hjorth, J., et al. 2003a, *A&A*, 400, 127
- Gorosabel, J., Klose, S., Christensen, L., et al. 2003b, *A&A*, 409, 123
- Greiner, J., Peimbert, M., Estaban, C., et al. 2003, *GRB Circular Network*, 2020, 1
- Hjorth, J., Holland, S., Courbin, F., et al. 2000, *ApJ*, 534, L147
- Hjorth, J., Sollerman, J., Møller, P., et al. 2003, *Nature*, 423, 847
- Hjorth, J., Thomsen, B., Nielsen, S. R., et al. 2002, *ApJ*, 576, 113
- Holland, S. T., Weidinger, M., Fynbo, J. P. U., et al. 2003, *AJ*, 125, 2291
- Infante, L., Garnavich, P. M., Stanek, K. Z., & Wyrzykowski, L. 2001, *GRB Circular Network*, 1152
- Jensen, B. L., Fynbo, J. U., Gorosabel, J., et al. 2001, *A&A*, 370, 909
- Kennicutt, R. C. 1998, *ARA&A*, 36, 189
- Landolt, A. U. 1992, *AJ*, 104, 372
- Le Flocc'h, E., Duc, P.-A., Mirabel, I. F., et al. 2003, *A&A*, 400, 499
- Lee, B. C., Tucker, D. L., Vanden Berk, D. E., et al. 2001, *ApJ*, 561, 183
- Leitherer, C., Schaerer, D., Goldader, J. D., et al. 1999, *ApJS*, 123, 3
- Lilly, S. J., Tresse, L., Hammer, F., Crampton, D., & Le Fevre, O. 1995, *ApJ*, 455, 108
- Miller, G. E. & Scalo, J. M. 1979, *ApJS*, 41, 513
- Odehahn, S. C., Djorgovski, S. G., Kulkarni, S. R., et al. 1998, *ApJ*, 509, L5
- Osterbrock, D. E. 1989, *Astrophysics of Gaseous Nebulae and Active Galactic Nuclei (Mill Valley: University Science Books)*
- Piro, L., Frail, D. A., Gorosabel, J., et al. 2002, *ApJ*, 577, 680
- Prevot, M. L., Lequeux, J., Prevot, L., Maurice, E., & Rocca-Volmerange, B. 1984, *A&A*, 132, 389
- Sahu, K. C., Vreeswijk, P., Bakos, G., et al. 2000, *ApJ*, 540, 74
- Salpeter, E. E. 1955, *ApJ*, 121, 161
- Schlegel, D. J., Finkbeiner, D. P., & Davis, M. 1998, *ApJ*, 500, 525
- Seaton, M. J. 1979, *MNRAS*, 187, 73P
- Sokolov, V. V., Fatkhullin, T. A., Castro-Tirado, A. J., et al. 2001, *A&A*, 372, 438
- Stanek, K. Z., Garnavich, P. M., Jha, S., et al. 2001, *ApJ*, 563, 592
- Stanek, K. Z., Matheson, T., Garnavich, P. M., et al. 2003, *ApJ*, 591, L17

- Vreeswijk, P. M., Fender, R. P., Garrett, M. A., et al. 2001b, A&A, 380, L21
- Vreeswijk, P. M., Fruchter, A., Kaper, L., et al. 2001a, ApJ, 546, 672
- Waxman, E. & Draine, B. T. 2000, ApJ, 537, 796
- Wijers, R. A. M. J., Bloom, J. S., Bagla, J. S., & Natarajan, P. 1998, MNRAS, 294, L13
- Woosley, S. E. 1993, ApJ, 405, 273